Are Semiclassical Methods Accurate for Electronically Nonadiabatic Transitions between Weakly Coupled Potential Energy Surfaces?

3 AUTHORS, INCLUDING:

Donald Truhlar
University of Minnesota Twin Cities

1,342 PUBLICATIONS   **81,158** CITATIONS

SEE PROFILE

Are Semiclassical Methods Accurate for Electronically Nonadiabatic Transitions between Weakly Coupled Potential Energy Surfaces?

Yuri L. Volobuev, Michael D. Hack, and Donald G. Truhlar*

Department of Chemistry and Supercomputer Institute, University of Minnesota, Minneapolis, Minnesota 55455-0431

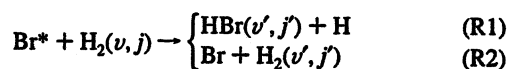Received: February 3, 1999; In Final Form: May 19, 1999

We have performed a systematic series of semiclassical and quantum mechanical calculations of collisions of Br* (electronicaly excited Br) with H_2 in order to test four semiclassical methods against accurate quantum mechanical scattering calculations for the quenching probability and the electronically nonadiabatic reaction probability. The results are analyzed using four different methods of assigning final quantum numbers based on the final values of the semiclassical and classical trajectory variables, namely energy-nonconserving histogram analysis, energy-conserving histogram analysis, energy-nonconserving linear smooth sampling, and energy-conserving linear smooth sampling. We examine the use of both forward and reverse state-to-state probabilities to predict the quenching and reaction probabilities. The reaction and quenching probabilities are compared to the results of accurate quantum mechanical calculations, and the mean unsigned error is calculated for each combination of a semiclassical method and a final analysis algorithm. Our results indicate that Tully's fewest switches (TFS) trajectory-surface-hopping method and the Ehrenfest self-consistent-potential method show the best agreement with the accurate results, although none of the methods provides satisfactory agreement in the cases where the reaction or quenching probability is small. The TFS method is the only one that can be used to calculate the reaction probabilities for this system directly in the forward direction, and it is judged to be the best method overall for weakly coupled potential energy surfaces.

1. Introduction

There is considerable interest in developing mixed quantal—classical methods for modeling the dynamics of electronically nonadiabatic molecular processes because such methods can be applied more readily than fully quantal techniques to the study of complex processes involving large molecules.[1] Comparison of various approaches to accurate quantal benchmarks is an important step in appraising their usefulness. In a recent paper,[2] four semiclassical methods[3–7] were tested against accurate quantal results[2,8,9] for three atom—diatom reactions involving conical intersections. The present paper extends that study to a qualitatively different kind of system, namely an atom—diatom reaction in which the diabatic potential surfaces do not cross but are approximately parallel in the entrance channel; this is sometimes called the Rosen—Zener—Demkov[10–12] case. The same four semiclassical methods are tested against accurate quantal results.

2. System

The system under study is

Figure 1. Potential energy curves for Br* + H_2 and Br + H_2 along the minimum energy path of the lowest adiabatic surface for the reaction Br* + H_2 → HBr + H from reactants to products. The left side of the figure corresponds to Br or Br* approaching or receding from H_2, and the right side corresponds to HBr far from H. The horizontal dashed lines denote the total energies of the collisions studied in this article, i.e., E_{tot} = 1.3 and 1.5 eV.

$$Br^* + H_2(v,j) \rightarrow \begin{cases} HBr(v',j') + H & \text{(R1)} \\ Br + H_2(v',j') & \text{(R2)} \end{cases}$$

where the asterisk (*) denotes electronic excitation, v and j are vibrational and rotational quantum numbers, and primes denote final values. Figure 1 shows the diabatic and adiabatic potential curves along the reaction path for the adiabatic reaction Br + H_2 → HBr + H. The value of the off-diagonal Hamiltonian matrix element U_{12} in the diabatic representation is constant for the potential matrix[13,14] used here and is equal to 0.215 eV.
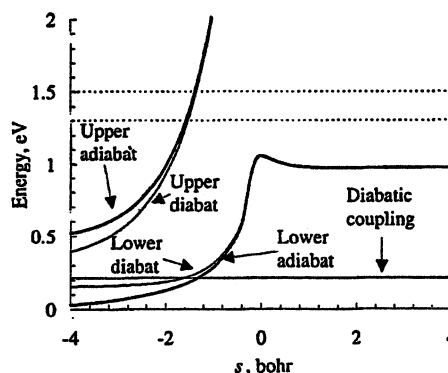
The diabatic potential energy surfaces are given in a previous paper.[13] The zero of energy corresponds to the adiabatic potential energy of Br infinitely separated from H_2 at its equilibrium separation. The adiabatic potential energies of Br* + H_2 and of HBr + H are 0.457 and 0.976 eV, respectively.

Process R1 is the nonadiabatic reaction and process R2 is nonreactive de-excitation. We will reserve the word "quenching" for the latter. The sum of the probabilities for nonadiabatic reaction and quenching is called the total nonadiabatic probability.

6226 *J. Phys. Chem. A, Vol. 103, No. 31, 1999*

Volobuev et al.

3. Dynamics Methods

3.1. Accurate Quantum Mechanics. The methods used for the accurate quantal calculations have been explained elsewhere. We used the hybrid-basis-set scattered wave variational principle[15,16] with S matrix boundary conditions[15] (which is also called the outgoing wave variational principle), as extended to electronically nonadiabatic rearrangement scattering.[17,18] Calculations on the present system require the definition of a vibronic asymptotically diagonal representation[14] because the coupling does not vanish in either the adiabatic or diabatic representation in the asymptotic region where boundary conditions are applied.

3.2. Semiclassical Calculations. The methods used for the semiclassical calculations are summarized in a previous paper.[2] We used four semiclassical methods:

1. MM: the Meyer–Miller method[3]
2. E: the Ehrenfest method with unbundled trajectories,[3] also called the quantum/classical time-dependent self-consistent field-method[6]
3. BT: the Blais–Truhlar trajectory-surface-hopping method[4]
4. TFS: Tully's fewest-switches trajectory-surface-hopping method[5]

The MM and E methods are called self-consistent-potential (SCP) methods, and the BT and TFS methods are called trajectory-surface-hopping (TSH) methods. The MM and E methods are independent of whether propagation is carried out in the adiabatic or diabatic representation, but we use the diabatic representation. The TFS calculations were carried out in the adiabatic representation, as recommended by Tully.[1,7]

Each of these four methods is applied with four different schemes for assigning probabilities to discrete final quantum states on the basis of the continuous final values of the semiclassical and classical trajectory variables. In particular, we used the histogram (H) method[19] and linear smooth sampling[20,21] (LSS), and each of these was applied in two ways. The first way, called energy nonconserving (ENC), accepts predictions of final-state populations even if the quantized state is not accessible with conservation of total energy. The second way, called energy conserving (EC), recognizes such predictions as excluded and uses algorithms[2] presented previously to reassign any such populations predicted by the semiclassical methods to the nearest energetically allowed discrete states. One of the purposes of the present paper is to test which of these schemes (ENC or EC) performs better. All four combinations, H–ENC, LSS–ENC, H–EC, and LSS–EC, are completely explained in our previous paper.[2] Note that final states of H_2 are always assigned even values of j since this paper is only concerned with para-H_2. Thus for both histogram and smooth sampling methods, and for both forward and reverse trajectories, we are always treating H_2 using j' bins that are two quanta wide.

Although the final-state analysis was discussed in a previous paper, we think it is useful to mention some further details of the calculation of the final vibrational quantum number in SCP methods, and this discussion is presented in Appendix A.

In previous work we have applied two variations of the TFS method: TFS-d and TFS-g. These two variations differ in the way the momenta are adjusted after a successful hop. In the TFS-d method, the momenta are adusted in the direction of the nonadiabatic coupling vector **d**; this is the approach used in the original TFS method[5] and has been justified theoretically by Herman[22] and Coker and Xiao.[23] In the TFS-g method, the momenta is adjusted in the direction of the gradient **g** of the energy gap between the initial and the final electronic states. In Appendix B we show that if the diabatic coupling is a

constant, as it is for the potential energy matrix[13,18] used here, the TFS-g and TFS-d methods are identical. Therefore we do not need the d and g labels for TFS methods in the present paper.

One final option concerns the direction in which the trajectories are run. None of these four semiclassical methods satisfies microscopic reversibility, so the classical transition probability $P_{kk'}$ for a $k \rightarrow k'$ transition is not equal to the transition probability for a $k' \rightarrow k$ transition, as it should be. In this paper all results are presented for the processes in the order they are written in section 2. When these forward results are obtained by running the trajectories backward, they are labeled reverse (R), e.g., reverse TFS (R-TFS) or reverse Ehrenfest (R-E). Backward trajectories differ from forward trajectories because backward trajectories are quantized for products but not for reactants, whereas forward trajectories are correctly quantized for reactants but not for products. Reverse trajectory methods have been well studied in the electronically adiabatic case.[24–26] Even when it is not known whether the reverse results are more accurate than the forward ones, they serve a useful role as a diagnostic since any large deviations between the forward and reverse results should be considered as a warning that perhaps neither is reliable.[19]

4. Calculations

All calculations in this paper are for total angular momentum J equal to zero. Therefore there is one quantum mechanical channel associated with each quantum state of the separated atom–diatom system in each arrangement. A state k is therefore specified by four quantum numbers α, n, v, and j where α is arrangement (it denotes which of the three atoms is separated from the other two when the atoms are numbered in the order H(1), Br(2), H(3), i.e., $\alpha = 1$ or 3 for the products of (R1), and $\alpha = 2$ for reactants and for the products of (R2)), n is electronic quantum number (2 for the excited state, 1 for the ground state), v is vibrational quantum number (0, 1, 2), and j is rotational quantum number (0, 1, ..., 18 for $\alpha = 1$ and 0, 2, ..., 12 for $\alpha = 2$). We use the convention that k denotes α, n, v, and j, and k' denotes α', n', v', and j'.

4.1. Definitions of Probabilities. We define the state-selected reaction probability of Br* with H_2 as

$$P_k^{react} = \sum_{k' \in (R1)} P_{kk'} \tag{1}$$

where k denotes a vibration–rotation state (v, j) of the reactants, and the sum is over all vibration–rotation states (v', j') of the HBr product of process (R1); thus the sum over k' includes both of the reactive arrangements (reaction with either H of H_2). We define the state-selected quenching probability as

$$P_k^{quench} = \sum_{k' \in (R2)} P_{kk'} \tag{2}$$

where k has the same meaning as in eq 1, but now the sum is over all vibration–rotation states of H_2 molecules produced with quenched Br according to process (R2). Finally we define the state-specific probability of a nonadiabatic collision as

$$P_k^{nonadiabatic} = P_k^{react} + P_k^{quench} \tag{3}$$

When reverse trajectories are used to calculate any of these quantities, one must start trajectories in every product state k', calculate $P_{k'k}$ by the H–ENC, LSS–ENC, H–EC, or LSS–

Study of Electronically Nonadiabatic Transitions

J. Phys. Chem. A, Vol. 103, No. 31, 1999 **6227**

TABLE 1: Nonreactive De-excitation (i.e., Quenching) Probabilities and Mean Unsigned Errors[a] Calculated by Quantum Scattering Calculations and by SCP Methods with Linear Smooth Sampling for Br* + $H_2(v,j)$ → Br + H_2 at $E_{tot} = 1.5$ eV

(v,j)	quantum	Meyer–Miller		Ehrenfest	
		ENC	EC	ENC	EC
(0,0)	1.4e−3	8.2e−3	8.2e−3	6.4e−4	6.4e−4
(0,2)	1.5e−3	1.6e−2	1.6e−2	2.5e−3	2.5e−3
(0,4)	4.4e−3	4.0e−2	4.0e−2	4.4e−3	4.4e−3
(0,6)	6.3e−3	2.5e−2	2.6e−2	2.6e−3	2.6e−3
(0,8)	4.3e−4	3.3e−2	3.5e−2	1.5e−3	1.6e−3
(0,10)	1.7e−7	1.6e−3	1.6e−3	8.1e−6	5.9e−1
(1,0)	1.4e−3	3.9e−2	4.5e−2	7.3e−3	7.4e−3
(1,2)	1.3e−2	9.4e−2	1.2e−1	1.2e−2	1.3e−2
(1,4)	4.2e−3	6.2e−2	7.2e−2	2.0e−2	9.1e−1
ΔP^{quench}		3.2e−2	3.7e−2	3.3e−3	1.7e−1

[a] Equation 5.

TABLE 2: Nonreactive De-excitation (i.e., Quenching) Probabilities and Mean Unsigned Errors Calculated by Quantum Scattering Calculations and by the TFS Method for Br* + $H_2(v,j)$ → Br + H_2, Summed over Final Vibrational−Rotational States

(v,j)	$E_{tot} = 1.3$ eV			$E_{tot} = 1.5$ eV		
	quantum	TFS[a]		quantum	TFS[a]	
		ENC	EC		ENC	EC
(0,0)	1.7e−3	2.0e−3	1.7e−3	1.4e−3	9.9e−4	9.3e−4
(0,2)	4.4e−3	2.2e−3	1.8e−3	1.5e−3	3.8e−3	3.7e−3
(0,4)	8.0e−3	7.0e−3	6.6e−3	4.4e−3	6.5e−3	6.3e−3
(0,6)	2.0e−3	3.2e−3	3.0e−3	6.3e−3	4.0e−3	4.1e−3
(0,8)	2.1e−2	4.3e−3	4.3e−3	4.3e−4	3.2e−3	3.4e−3
(0,10)[b]	–	–	–	1.7e−7	1.5e−4	1.0e+0
(1,0)	2.1e−6	2.3e−3	2.2e−3	1.4e−3	7.3e−3	7.0e−3
(1,2)	9.5e−6	5.4e−4	3.2e−4	1.3e−2	1.3e−2	1.1e−2
(1,4)[b]	–	–	–	4.2e−3	2.0e−2	7.5e−1
ΔP^{quench}		3.5e−3	3.5e−3		3.5e−3	2.0e−1

[a] For the TFS method, the histogram and linear smooth sampling methods give identical reactive and quenching probabilities when summed over final vibrational−rotational states. [b] At $E_{tot} = 1.3$ eV states (0,10) and (1,4) are closed.

TABLE 3: Branching Ratios Calculated by Quantum Scattering Calculations and by the Forward TFS Method for Br* + $H_2(v,j)$ Using the Formula $P^{react}/(P^{react} + P^{quench})$

(v,j)	$E_{tot} = 1.3$ eV			$E_{tot} = 1.5$ eV		
	quantum	TFS[a]		quantum	TFS[a]	
		ENC	EC		ENC	EC
(0,0)	0.279	0.099	0.115	0.323	0.353	0.367
(0,2)	0.248	0.191	0.224	0.462	0.205	0.209
(0,4)	0.138	0.136	0.143	0.276	0.207	0.222
(0,6)	0.101	0.179	0.189	0.136	0.310	0.328
(0,8)	0.000	0.034	0.034	0.571	0.192	0.183
(0,10)[b]	–	–	–	0.144	0.051	0.000
(1,0)	0.000	0.019	0.020	0.667	0.112	0.116
(1,2)	0.000	0.025	0.042	0.187	0.240	0.272
(1,4)[b]	–	–	–	0.005	0.174	0.006

[a] For the TFS method, the histogram and linear smooth sampling methods give identical reactive and quenching probabilities. [b] At $E_{tot} = 1.3$ eV states (0,10) and (1,4) are closed.

EC algorithm, set $P_{kk'}$ equal to $P_{k'k}$, and then sum over k'. Furthermore, most of the reverse trajectories have low translational energy, which increases the computational cost by about an order of magnitude. Thus the reverse trajectory methods require considerably more computation than the forward methods. Of course it is not necessary to run trajectories starting in arrangement 3 since these results are identical to those starting in arrangement 1 by symmetry; thus one actually carries out
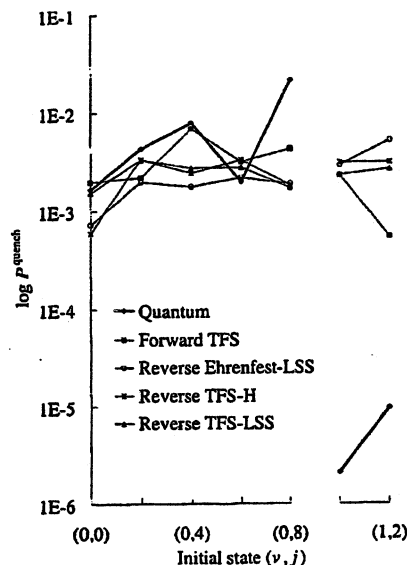

Figure 2. Nonreactive de-excitation (i.e., quenching) probabilities calculated by quantum mechanical scattering calculations and by various semiclassical methods for Br* + $H_2(v,j)$ → Br + H_2, summed over final vibrational−rotational states, at $E_{tot} = 1.3$ eV. Energy conservation was not enforced. For the TFS method, the histogram and linear smooth sampling algorithms give identical quenching probabilities when summed over final vibrational−rotational states.

TABLE 4: Branching Ratios Calculated by Quantum Scattering Calculations and by the Reverse Methods for Br* + $H_2(v,j)$ at $E_{tot} = 1.3$ eV Using the Formula $P^{react}/(P^{react} + P^{quench})$

(v,j)	quantum	reverse TFS				reverse Ehrenfest	
		histogram		LSS		LSS	
		ENC	EC	ENC	EC	ENC	EC
(0,0)	0.279	0.000	0.000	0.006	0.006	0.011	0.011
(0,2)	0.248	0.038	0.038	0.134	0.160	0.033	0.033
(0,4)	0.138	0.178	0.178	0.209	0.241	0.197	0.197
(0,6)	0.101	0.194	0.194	0.161	0.155	0.167	0.166
(0,8)	0.000	0.000	0.000	0.004	0.006	0.050	0.049
(1,0)	0.000	0.000	0.000	0.003	0.003	0.024	0.026
(1,2)	0.000	0.389	0.389	0.351	0.387	0.309	0.339

the reverse trajectory calculations for process R1 starting in the $\alpha = 1$ arrangement and multiplying the result by 2 to account for this fact.

4.2. Specifics of the Calculations and Results. We performed forward calculations for 11 different states k at a total energy E of 1.5 eV, and we performed both forward and reverse calculations for 8 different states k at $E = 1.3$ eV.

All quantal results in this paper were carried out using basis set A2 given in the supporting information of ref 14 and version 18.7 of the VP computer code[27] on an SGI Origin2000 computer. For quantities published previously,[13,14] we obtained essentially the same results as before for reaction and quenching probabilities greater than 10^{-4}.

The semiclassical calculations were carried out first using version 5.3 of the TSH computer code[28] on an IBM SP computer; this code uses the Bulirsch-Stoer method to integrate the coupled differential equations. For the TFS method, we checked the accuracy of the Bulirsch-Stoer method[29] by using version 5.5 of the TSH code, which uses an improved integration algorithm.[30] We found that in all cases the difference between the results of two integration methods was less than the standard deviation due to the Monte Carlo sampling statistics.
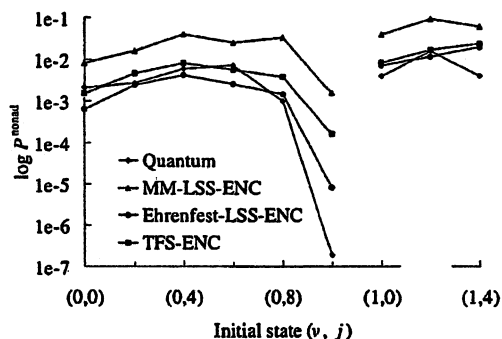
Figure 3. Nonadiabatic probabilities calculated by quantum mechanical scattering calculations and by various semiclassical methods for Br* + $H_2(v, j)$ at $E_{tot} = 1.5$ eV. All results in this figure are for forward methods.
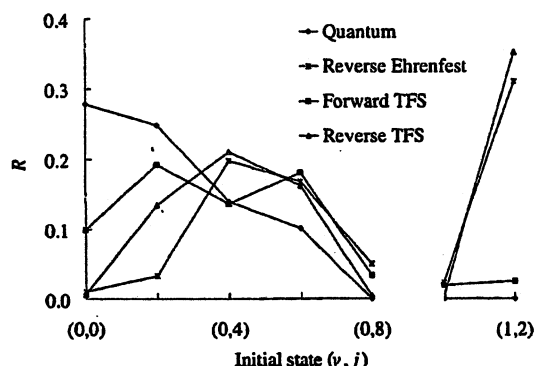

Figure 4. Branching ratios calculated by quantum scattering calculations and by the forward and reverse semiclassical methods for Br* + $H_2(v, j)$ at $E_{tot} = 1.3$ eV using the formula $R = P^{react}/(P^{react} + P^{quench})$. All results in this figure are based on linear smooth sampling, and energy conservation was not enforced.

For the forward SCP methods, 50 000 trajectories were computed for each initial state. For the TFS method, we used a different number of trajectories for different initial states: for the states where the reaction probability (calculated from a test batch of 50 000 trajectories) is larger than 0.001, no more trajectories were calculated, thus leaving the total at 50 000 trajectories per initial state; for the initial states where the reaction probability is between 0.0001 and 0.001, an additional 150 000 trajectories were calculated, for a total of 200 000 per state; for all other states an additional 450 000 trajectories were calculated, for a total of 500 000 per state. For the reverse Ehrenfest and reverse TFS calculations on (R1), 30 000 and 15 000 trajectories, respectively, were computed for each of the 12 different initial states ($v' = 0$, $j' = 0-11$). For the reverse Ehrenfest and reverse TFS calculations on (R2), 15 000 trajectories were computed for each of the 12 different initial states ($v' = 0-2$, $j' = 0-12$, even j states only).

The full set of quantal and semiclassical values of $P_{kk'}$ for reactions R1 and R2 and for the probabilities defined in eqs 1–3 are given in Tables 1–4 of this paper and Tables S-1 to S-20 of the Supporting Information,[29] and representative results are illustrated in Figures 2–4. Some of the probabilities are not tabulated or shown on figures, specifically:

(a) The BT method never predicts any reaction or quenching; therefore none of the BT results are presented in detail. An attempt was made to modify the BT method so that it can predict small probabilities. The new method, however, does not give stable results (see Appendix C).

TABLE 5: Mean Unsigned Errors for Various Semiclassical Methods for Br* + H_2 at $E_{tot} = 1.3$ eV

method	analysis	ΔP^{quench}	ΔP^{nonad}	ΔP^{react}	ΔP_{av}
MM	H–ENC	0.0054	0.0059	0.0005	0.0039
	LSS–ENC	0.0167	0.0162	0.0005	0.0111
	H–EC	0.0054	0.0059	0.0005	0.0039
	LSS–EC	0.0178	0.0173	0.0005	0.0119
Ehrenfest	H–ENC	0.0054	0.0059	0.0005	0.0039
	LSS–ENC	0.0041	0.0046	0.0005	0.0031
	H–EC	0.0054	0.0059	0.0005	0.0039
	LSS–EC	0.0041	0.0046	0.0005	0.0031
BT	any	0.0054	0.0059	0.0005	0.0039
TFS	H–ENC	0.0035	0.0037	0.0003	0.0025
	LSS–ENC	0.0035	0.0037	0.0003	0.0025
	H–EC	0.0035	0.0038	0.0003	0.0025
	LSS–EC	0.0035	0.0038	0.0003	0.0025
R-Ehrenfest	H–ENC	0.0054	0.0059	0.0005	0.0039
	LSS–ENC	0.0054	0.0061	0.0008	0.0041
	H–EC	0.0054	0.0059	0.0005	0.0039
	LSS–EC	0.0054	0.0063	0.0009	0.0042
R-BT	any	0.0054	0.0059	0.0005	0.0039
R-TFS	H–ENC	0.0050	0.0057	0.0008	0.0038
	LSS–ENC	0.0046	0.0051	0.0006	0.0034
	H–EC	0.0050	0.0057	0.0008	0.0038
	LSS–EC	0.0045	0.0050	0.0005	0.0034

(b) For SCP methods (Miller–Meyer and Ehrenfest) the histogram method always results in zero reaction and quenching probabilities. Only LSS results are tabulated.

(c) Forward SCP or reverse histogram SCP methods always result in zero probability for the reaction R1; therefore for the forward SCP methods only the quenching probabilities are tabulated and no probabilities are tabulated for the reverse histogram SCP methods.

Since there are too many probabilities to discuss them all in detail, we will concentrate on understanding the trends. To obtain an overview of the results, we calculated a mean unsigned error for each method as follows:

$$\Delta P_{av}(E) = \frac{\Delta P^{react}(E) + \Delta P^{quench}(E) + \Delta P^{nonad}(E)}{3} \quad (4)$$

where each of the three quantities on the right-hand side is defined as follows:

$$\Delta P^X(E) = \frac{1}{N} \sum_{k=1}^{N} |P_k^X(E,\text{semiclassical}) - P_k^X(E,\text{quantal})| \quad (5)$$

where N is the number of k states considered at energy E. The overall mean unsigned error for the forward methods was defined as

$$\Delta P = \frac{\Delta P_{av}(E_{tot}=1.3 \text{ eV}) + \Delta P_{av}(E_{tot}=1.5 \text{ eV})}{2} \quad (6)$$

These overall mean unsigned errors are given for all methods in Tables 5–7.

We also tested a forward/reverse combined method in which

$$P_{kk'} = \begin{cases} P_{kk'}^{forward} & \text{if } E_k > E_{k'} \\ P_{kk'}^{reverse} & \text{if } E_{k'} > E_k \end{cases}$$

where E_k is the internal energy in state k. This is a simplified version of a method suggested by Ashton et al.[25] The errors for this method were between those for the pure forward and reverse

Study of Electronically Nonadiabatic Transitions

J. Phys. Chem. A, Vol. 103, No. 31, 1999 **6229**

TABLE 6: Mean Unsigned Errors for Various Semiclassical Methods for Br* + H$_2$ at E_{tot} = 1.5 eV

method	analysis	ΔP^{quench}	ΔP^{nonad}	ΔP^{react}	ΔP_{av}
MM	H−ENC	0.0036	0.0048	0.0012	0.0032
	LSS−ENC	0.0318	0.0306	0.0012	0.0212
	H−EC	0.0036	0.0048	0.0012	0.0032
	LSS−EC	0.0368	0.0356	0.0012	0.0245
Ehrenfest	H−ENC	0.0036	0.0048	0.0012	0.0032
	LSS−ENC	0.0033	0.0035	0.0012	0.0027
	H−EC	0.0036	0.0048	0.0012	0.0032
	LSS−EC	0.1676	0.1679	0.0012	0.1122
BT	any	0.0036	0.0048	0.0012	0.0032
TFS	H−ENC	0.0035	0.0038	0.0010	0.0028
	LSS−ENC	0.0035	0.0038	0.0010	0.0028
	H−EC	0.1959	0.1960	0.0010	0.1309
	LSS−EC	0.1959	0.1960	0.0010	0.1309
R-BT	any	0.0036	0.0048	0.0012	0.0032

TABLE 7: Overall Mean Unsigned Errors ΔP_{av} and ΔP for the Forward and Reverse Methods

		forward		reverse[a]
	analysis	both E	E = 1.3 eV	E = 1.3 eV
MM	H−ENC	0.0036	0.0039	b
Ehrenfest	H−ENC	0.0036	0.0039	0.0039
BT	H−ENC	0.0036	0.0039	0.0039
TFS	H−ENC	0.0026	0.0025	0.0038
MM	LSS−ENC	0.0162	0.0111	b
Ehrenfest	LSS−ENC	0.0029	0.0031	0.0041
BT	LSS−ENC	0.0036	0.0039	0.0039
TFS	LSS−ENC	0.0026	0.0025	0.0034
MM	H−EC	0.0036	0.0039	b
Ehrenfest	H−EC	0.0036	0.0039	0.0039
BT	H−EC	0.0036	0.0039	0.0039
TFS	H−EC	0.0667	0.0025	0.0038
MM	LSS−EC	0.0182	0.0119	b
Ehrenfest	LSS−EC	0.0577	0.0031	0.0042
BT	LSS−EC	0.0036	0.0039	0.0039
TFS	LSS−EC	0.0667	0.0025	0.0034

[a] For the reverse methods, calculations were done only at E_{tot} = 1.3 eV. [b] Reverse MM calculations were not done.

TABLE 8: Mean Unsigned Errors in Total Nonadiabatic Probability Averaged over Both Energies[a]

method	ENC	EC
MM	0.0234	0.0265
Ehrenfest	0.0041	0.0862
Blais−Truhlar[b]	0.0054	0.0054
TFS	0.0038	0.0999

[a] Forward trajectories with LSS analysis. [b] P^{nonad} = 0 for this method for the system and energies studied in this paper.

methods, but usually closer to the less accurate reverse method, so we will not discuss this method any further.

5. Discussion

5.1. Quenching Probabilities. The SCP methods predict no quenching when histogram analysis is used. Table 1 shows the results obtained using SCP methods with LSS analysis at 1.5 eV; similar results are obtained at 1.3 eV and are given in Table S-1 of Supporting Information. The Meyer−Miller SCP method seriously overestimates the quenching probability; in more than half the cases the error is more than a factor of 10. The Ehrenfest method usually yields the correct order of magnitude, although for a few cases at 1.3 eV the errors are much larger.

For the TSH methods, histogram and LSS methods yield the same quenching probabilities if the results are summed over final vibrational−rotational states. The Blais−Truhlar method predicts no quenching. The results for Tully's fewest switches method are shown in Table 2. Usually, but not always, the results are the correct order of magnitude.

Table 5 and Figure 2 show that on average the reverse methods are slightly worse. Tables 5 and 6 show that the best method, on average, for quenching probabilities is Tully's fewest switches method in the forward direction at 1.3 eV and Ehrenfest's method with LSS analysis and not forcing energy conservation at 1.5 eV. It is somewhat discouraging though that the average improvement of the very best methods over the methods that simply predict zero (e.g., SCP histogram methods

or the Blais−Truhlar method) is only 33% (0.36 vs 0.54) at 1.3 eV and 8% (0.33 vs 0.36) at 1.5 eV. Furthermore, Table 6 shows that the best method at 1.5 eV (Ehrenfest−LSS) becomes much worse if one reassigns final states that violate energy conservation; this result indicates that the small average error of the Ehrenfest−LSS method is achieved in a somewhat nonphysical manner by populating disallowed states.

5.2. Total Nonadiabatic Probability. In judging methods for treating collisions of electronically excited atoms, it is of interest to consider their accuracy for the total probability of de-excitation, independent of whether or not the system reacts. Since histogram analysis predicts no de-excitation for SCP methods and the same amount of de-excitation as linear smooth sampling for TSH methods, and since Table 5 shows that reverse methods are less accurate, on average, than forward methods for the total nonadiabatic probability, we will discuss only forward linear smooth sampling results. Figure 3 and Tables 5 and 6 show that, just as for quenching probabilities, Tully's fewest switches method is most accurate at 1.3 eV, and the Ehrenfest method is most accurate at 1.5 eV, whether or not energy conservation is not enforced, but both of these methods become less accurate at 1.5 eV if energy conservation is required in the final-state analysis. Averaging the mean error ΔP^{nonad} over the two energies gives the results shown in Table 8. The Meyer−Miller method is unsuccessful, with average errors more than a factor of 4 greater than the average probability, and the Ehrenfest and Tully's fewest switches methods are most accurate, with average errors smaller than the average probability. The results for the Blais−Truhlar method are shown just as a point of reference; clearly the average error equals the average probability for this method.

5.3. Reaction Probabilities. The Meyer−Miller, Ehrenfest, and Blais−Truhlar methods predict no nonadiabatic reaction in the forward direction, and the Blais−Truhlar method predicts no nonadiabatic reaction even with reverse trajectories. The reactive branching ratios for Tully's fewest switches method with forward or reverse trajectories and for the Ehrenfest method with reverse trajectories are shown in Tables 3 and 4 and in Figure 4. None of the methods gets the trends completely right, although Tully's forward method comes closest. As pointed out in section 3.2, though, when the results based on forward and reverse trajectories differ significantly, as they do here, it is an indication that the method is unreliable. (In particular, it does not occur because we have too few trajectories. The trends are different and would remain different even if we improved the statistics further.)

Reverse methods are expensive (because we must run a full set of trajectories for each final state, most of which have low translational energy, rather than just for a single initial state), and although the results are only slightly worse than forward methods, that may be fortuitous. Some of the state-to-state reaction probabilities for reverse methods are very inaccurate. Final-state analysis clearly shows that energy conservation is of great importance when dealing with the reverse methods, more so than for the forward methods, but the present energy

6230 *J. Phys. Chem. A, Vol. 103, No. 31, 1999*

Volobuev et al.

conservation algorithm does not improve the agreement with the quantum results.

The average errors in the reaction probabilities are shown in Tables 5 and 6. Tully's fewest switches method is the best, and the average error is 40% (1.3 eV) or 25% (1.5 eV) better than for the methods that predict no reaction.

Both SCP methods predict zero reaction probability in the forward direction. Reverse methods do not provide overall improvement in the error. Even if reverse methods did work well, the cost of the computation is about 2 orders of magnitude more than for forward calculations. The cost of a reverse calculation grows very rapidly with the total energy, as more final states become open. (Since trajectory results are usually smooth functions of rotational quantum numbers, one could bring the cost of reverse calculations down by running only selected rotational states and interpolating, but that was not done here.)

5.4. Overall Error. Table 7 shows that the overall errors, which were defined in eq 6, are smallest for the Ehrenfest and Tully's fewest switches methods when energy conservation is not enforced, but are nevertheless disappointingly large. The Blais–Truhlar method predicts no nonadiabatic transition for a weakly coupled system like the present example, so its average error equals the average probability and is presented only as a benchmark for the other methods to strive to better. Table 7 shows that they do indeed perform better but only by predicting nonphysical transitions into energetically closed states. When the final states in such cases are reassigned to the closest energetically allowed state of that arrangement by the systematic method of ref 2, the overall average error actually exceeds the average probability. One does better by taking all nonadiabatic probabilities as zero, which caps the unsigned error at 100%. One would still prefer the methods that predict nonzero probabilities if they yielded useful trends or branching ratios, but the trends and branching ratios are not qualitatively correct whether or not one reassigns energetically forbidden final states.

Reverse methods are computationally expensive, but they do not agree any better than the forward methods with the accurate quantum calculations. Enforcing energy conservation using the present algorithm never improves the results, and it often makes them much worse.

Overall, the TFS–H–ENC and E–LSS–ENC methods work the best. The MM method does represent the correct trend, but it consistently overestimates the probabilities. None of the methods predicts small probabilities even qualitatively correctly, with the Ehrenfest method being the least inaccurate for nonreactive collisions. The TFS method is the best for reactive nonadiabatic collisions.

6. Conclusions

The TFS method is the best overall method for this system if energy conservation is not enforced. Ehrenfest is the second best; it is almost as good as TFS for the quenching probabilities, but it always predicts a zero reaction probability. Forcing energy conservation makes the results worse if it has an effect, and it has a more detrimental effect on the TFS method than the Ehrenfest one, so the Ehrenfest method has the smallest average error if one insists on energy conservation. Reverse methods are much more expensive than forward ones, but their accuracy is no better than the direct methods. In general the results are not encouraging for our ability to make reliable quantitative semiclassical calculations on photochemical reactions in which the potential surfaces are weakly coupled, but the fewest-

switches trajectory-surface-hopping method is fairly robust for usually predicting the correct order of magnitude.

Supporting Information Available: Tables S-1 to S-20 contain additional transition probabilities from the semiclassical and quantum mechanical calculations (20 pages). This material is available free of charge via the Internet at http://pubs.acs.org.

Appendix A

A critical step in the final-state analysis[2] is the calculation of the classical (continuous, unquantized) vibrational action $I_{vib}(t_f)$ at the final trajectory time t_f. In trajectory-surface-hopping methods, a system is always propagating on one or another potential energy surface, which dissociates to a well-defined diatomic potential curve $V_m(r)$, where m labels the electronic state, and r is the diabatic internuclear distance. Then[2,19]

$$I_{vib}(t_f) = \oint dr \sqrt{2\mu_{diat}[E - T_{rel}(t_f) - V_{m,eff}]} \quad \text{(A-1)}$$

where the integration is over a full vibrational period, μ_{diat} is the diatomic reduced mass, E is total energy, $T_{rel}(t_f)$ is the final relative translational energy of the atom with respect to the diatom, and

$$V_{m,eff}(r,t_f) = V_m(r) + \frac{[J_{rot}(t_f)]^2}{2\mu_{diat}r^2} \quad \text{(A-2)}$$

where $J_{rot}(t_f)$ is the final magnitude of the classical rotational angular momentum. In SCP methods, though, the final electronic populations are n_1 for $m = 1$ and $(1 - n_1)$ for $m = 2$. Asymptotically n_1 becomes a constant, and the diatomic radial motion is governed by a mixed effective potential

$$V_{mix,eff}(r) = n_1 V_{1,eff}(r) + n_2 V_{2,eff}(r) \quad \text{(A-3)}$$

Then

$$I_{vib}(t_f) = \oint dr \sqrt{2\mu_{diat}[E - T_{rel}(t_f) - V_{mix,eff}(r)]} \quad \text{(A-4)}$$

This is evaluated as follows. The final diatomic radial kinetic energy is given by

$$T_{diat}(t_f) = E - T_{rel}(t_f) - V_{mix,eff}(r(t_f)) \quad \text{(A-5)}$$

Then

$$I_{vib}(t_f) = \oint dr \sqrt{2\mu_{diat}[T_{diat}(t_f) + V_{mix,eff}(t_f) - V_{mix,eff}(r)]} \quad \text{(A-6)}$$

We define

$$W(r) = V_{2,eff}(r) - V_{1,eff}(r) \quad \text{(A-7)}$$

Then

$$I_{vib}(t_f) = \oint dr \,\{2\mu_{diat}[I_1(t_f,r) + I_2(t_f,r)]\}^{1/2} \quad \text{(A-8)}$$

where

$$I_1(t_f,r) = T_{diat}(t_f) + V_{1,eff}(t_f) + V_{1,eff}(r) \quad \text{(A-9)}$$

Study of Electronically Nonadiabatic Transitions

J. Phys. Chem. A, Vol. 103, No. 31, 1999 **6231**

and

$$I_2(t_f, r) = (1 - n_1)[W(t_f) - W(r)] \qquad (A\text{-}10)$$

Under two frequently encountered circumstances, $I_2(t_f)$ is zero or very small and can be neglected. First of all, this is true if $V_1(r)$ is parallel to $V_2(r)$. This is true at the (M or M*) + H_2 asymptotes in ref 2 (where M is a metal atom) or at the (Br or Br*) + H_2 asymptote in the present paper. The second circumstance where $I_2(t_f, r)$ can be neglected is when n_1 is very small or zero. This occurs at the MH + H asymptotes in ref 2 or at the HBr + H asymptote in the present paper.

Appendix B

Consider a diabatic potential energy matrix with constant coupling terms given by

$$V^d(R) = \begin{pmatrix} U_{11}(R) & U_{12} \\ U_{12} & U_{22}(R) \end{pmatrix} \qquad (B\text{-}1)$$

where

$$U_{ii}(R) = \langle \phi_i^d(x;R)|H_{el}(x;R)|\phi_i^d(x;R)\rangle \qquad (B\text{-}2)$$

$$U_{12} = \langle \phi_1^d(x;R)|H_{el}(x;R)|\phi_2^d(x;R)\rangle = \text{constant} \qquad (B\text{-}3)$$

and $H_{el}(x;R)$ is the electronic Hamiltonian (which also includes the nuclear Coulombic energy), R is the vector of nuclear coordinates, x is the vector of electronic coordinates, the integrations in eqs B-2 and B-3 are over x, and $\phi_i^d(x;R)$ and $\phi_j^d(x;R)$ are orthonormal diabatic states satisfying:

$$\langle \phi_i^d(x;R)|\nabla_R|\phi_j^d(x;R)\rangle = 0 \qquad (B\text{-}4)$$

$$\langle \phi_i^d(x;R)|\phi_j^d(x;R)\rangle = \delta_{ij} \qquad (B\text{-}5)$$

where ∇_R is the gradient over R and δ_{ij} is the Kronecker delta. As discussed elsewhere,[30] eq B-4 is possible only for certain model systems. In particular, as proposed by Preston and Tully,[31,32] it is possible for systems satisfying what we have called[30] the invariant-space approximation. The present system (like essentially all systems that have been treated by semiclassical and classical trajectory methods) satisfies this approximation by construction.

The diabatic potential matrix in eq B-1 can be diagonalized to give the adiabatic potential energy matrix:

$$V^a(R) = \begin{pmatrix} A_{11}(R) & 0 \\ 0 & A_{22}(R) \end{pmatrix} \qquad (B\text{-}6)$$

where

$$A_{11}(R) = \langle \phi_1^a(x;R)|H_{el}(x;R)|\phi_1^a(x;R)\rangle =$$
$$\bar{U}(R) - \sqrt{\Delta U(R)^2 + U_{12}^2} \qquad (B\text{-}7)$$

$$A_{22}(R) = \langle \phi_2^a(x;R)|H_{el}(x;R)|\phi_2^a(x;R)\rangle =$$
$$\bar{U}(R) + \sqrt{\Delta U(R)^2 + U_{12}^2} \qquad (B\text{-}8)$$

and

$$\bar{U}(R) = (1/2)(U_{22}(R) + U_{11}(R)) \qquad (B\text{-}9)$$

$$\Delta U(R) = (1/2)(U_{22}(R) - U_{11}(R)) \qquad (B\text{-}10)$$

and $\phi_1^a(x;R)$ and $\phi_2^a(x;R)$ are adiabatic states. These states can be expanded in the diabatic basis:

$$\phi_1^a(x;R) = c_{11}(R) \, \phi_1^d(x;R) + c_{12}(R) \, \phi_2^d(x;R) \qquad (B\text{-}11)$$

$$\phi_2^a(x;R) = c_{21}(R) \, \phi_1^d(x;R) + c_{22}(R) \, \phi_2^d(x;R) \qquad (B\text{-}12)$$

where

$$c_{11}(R) = -\frac{\Delta U(R) + \sqrt{\Delta U(R)^2 + 4U_{12}^2}}{N_1(R)} \qquad (B\text{-}13)$$

$$c_{12}(R) = \frac{2U_{12}}{N_1(R)} \qquad (B\text{-}14)$$

$$c_{21}(R) = -\frac{\Delta U(R) - \sqrt{\Delta U(R)^2 + 4U_{12}^2}}{N_2(R)} \qquad (B\text{-}15)$$

$$c_{22}(R) = \frac{2U_{12}}{N_2(R)} \qquad (B\text{-}16)$$

and

$$N_1(R) = \sqrt{4U_{12}^2 + (\Delta U(R) + \sqrt{\Delta U(R)^2 + U_{12}^2})^2} \qquad (B\text{-}17)$$

$$N_2(R) = \sqrt{4U_{12}^2 + (\Delta U(R) - \sqrt{\Delta U(R)^2 + U_{12}^2})^2} \qquad (B\text{-}18)$$

The nonadiabatic coupling vector is defined as

$$d_{12}(R) = \langle \phi_1^a(x;R)|\nabla_R|\phi_2^a(x;R)\rangle \qquad (B\text{-}19)$$

When eqs B-11 and B-12 are substituted into eq B-19, and the integration is carried out with eqs B-4 and B-5, the nonadiabatic coupling can be written:

$$d_{12}(R) = c_{12}(R)\nabla_R c_{22}(R) + c_{11}(R)\nabla_R c_{21}(R) \qquad (B\text{-}20)$$

which can be simplified to:

$$d_{12}(R) = \frac{1}{N_1(R) \, N_2(R)}\left[\frac{4U_{12}^2}{\sqrt{\Delta U(R)^2 + 4U_{12}^2}}\right]\nabla_R[U_{22}(R) - U_{11}(R)] \qquad (B\text{-}21)$$

It can be seen that $d_{12}(R)$ points in the direction of the difference of the gradients of the diabatic potential matrix elements $U_{11}(R)$ and $U_{22}(R)$. Note that the sign on $d_{12}(R)$ is arbitrary, in the usual way for off-diagonal matrix elements, since the adiabatic states defined in eqs B-10 and B-11 may be multiplied by a phase factor without changing the adiabatic potential in eq B-6.

Now consider the vector defined by

$$g_{12}(R) = \nabla_R[A_{22}(R) - A_{11}(R)] \qquad (B\text{-}22)$$

Substituting eqs B-7 and B-8 into eq B-22 gives a result that can be simplified to

$$g_{12}(R) = 2\nabla_R\sqrt{\Delta U(R)^2 + U_{12}^2} \qquad (B\text{-}23)$$

or to

$$g_{12}(R) = \frac{2\Delta U(R)}{\sqrt{\Delta U(R)^2 + U_{12}^2}} \nabla_R [U_{22}(R) - U_{11}(R)] \qquad (B\text{-}24)$$

Equation B-24 shows that the vector $g_{12}(R)$ also points in the direction of difference in the gradients of the diabatic potential matrix elements. The sign on $g_{12}(R)$, unlike the sign on $d_{12}(R)$, is well-defined.

The vectors $d_{12}(R)$ and $g_{12}(R)$ may be parallel for some geometries and antiparallel for others. Consider the angle, θ_{dg}, between $d_{12}(R)$ and $g_{12}(R)$:

$$\cos \theta_{dg} = \frac{g_{12}(R) \cdot d_{12}(R)}{|g_{12}(R)||g_{12}(R)|} = \text{sign}[\Delta U(R)] \quad (B\text{-}25)$$

Note that the sign of the dot product will change at the line of crossings between $U_{11}(R)$ and $U_{22}(R)$. On one side of this line, the two vectors will be parallel; on the other side they will be antiparallel. For potential matrices in which there are no crossings between $U_{11}(R)$ and $U_{22}(R)$, the vectors $d_{12}(R)$ and $g_{12}(R)$ will be parallel (or antiparallel) for all geometries. However, we note that the TFS methods are invariant to the sign on the unit vector that identifies the direction in which the momentum is incremented or decremented.

Appendix C

The generalized Blais–Truhlar (GBT) method is a modification of the original BT method that allows weakly coupled systems to be studied. This overcomes a disadvantage of the original BT method, which is that no hops will ever occur if the probability of being in the current electronic state never drops to 0.5.

The GBT method involves a parameter, ϵ_{BT}, that is between 0.0 and 0.5. If the probability of being in the current electronic state drops to $1 - \epsilon_{BT}$, then a quantum mechanical measurement is made. The trajectory hops with a probability of ϵ_{BT}, and remains in the current state with a probability of $1 - \epsilon_{BT}$. The trajectory is reinitialized in either case. Here reinitialization is taken to mean that the real part of the coefficient of one of the electronic states is set to equal 1, and the imaginary part of this coefficient and both parts of the remaining coefficients are set to be 0.

We choose ϵ_{BT} to be an order of magnitude smaller than the average change in the electronic probabilities, as computed from a small batch of trajectories in the absence of hopping events. This would allow the observation of hopping events even for systems in which the probability only changes by a very small amount. The hypothesis to be tested is whether the calculated value of the total quenching probability is independent of the parameter ϵ_{BT} over some range of values.

The quenching probability for BrH$_2$ as a function of ϵ_{BT} is shown in Figure 5. Note that there is no plateau region. At a high value of ϵ_{BT} the quenching probability, P_Q, is zero, as expected (notice that $\epsilon_{BT} = 0.5$ yields the original BT method exactly). As ϵ_{BT} decreases, the system experiences more hopping decisions, and P_Q increases. Past a certain point, however, P_Q decreases instead of reaching a stability region. We can explain this second trend by examining the form of the equations for the electronic coefficients whose square magnitude gives the probability of being in either adiabatic state. These equations are[1,5]

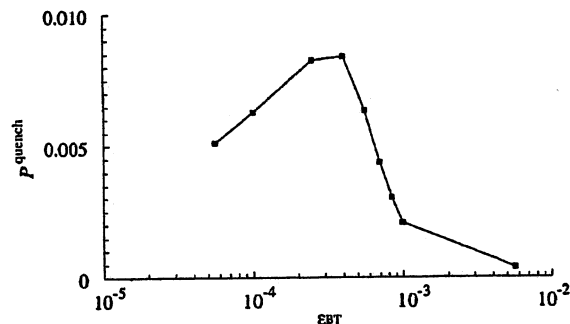$$\dot{c}_1 = -c_2 \dot{R} \cdot d_{12}(R) \qquad (C\text{-}1)$$

Figure 5. Dependence of the nonreactive de-excitation (i.e., quenching) probabilities calculated by generalized Blais–Truhlar method for Br* + H$_2$(0,0) → Br + H$_2$ on parameter ϵ_{BT}, at E_{tot} = 1.3 eV.

and

$$\dot{c}_2 = -c_1 \dot{R} \cdot d_{12}(R) \qquad (C\text{-}2)$$

where c_1 and c_2 are complex coefficients. The time derivatives of the probabilities of being in state 1 or 2 can be shown to be equal to

$$\dot{P}_2 = 2 \text{ Re}[c_2 {}^* c_1] \dot{R} \cdot d_{12}(R) \qquad (C\text{-}3)$$

and

$$\dot{P}_1 = -2 \text{ Re}[c_2 {}^* c_1] \dot{R} \cdot d_{12}(R) \qquad (C\text{-}4)$$

Thus, the rate of change of the probabilities depends coherently upon past history. Following a reinitialization, the coherence is zero, and the probabilities will be stationary. They will remain so until the coherence grows to some significant value, and, from eqs C-1 and C-2 we see that this rate of change is given by

$$\frac{\partial}{\partial t} \text{Re}[c_2 {}^* c_1] = (P_1 - P_2) \dot{R} \cdot d_{12}(R) \qquad (C\text{-}5)$$

Note that in the GBT method, as ϵ_{BT} is set to smaller and smaller values, measurement events occur more often. Regardless of whether a hop occurs or not, the trajectory is reinitialized. In a sense, we force the trajectories to exist in a regime where the probabilities are changing slowly, or not at all. In the limit of an infinitesimal value of ϵ_{BT}, the total number of hops approaches zero. This can be more clearly seen by examining an ideal case where $\dot{R} \cdot d_{12}(R) = 1$ at all geometries and all times. It can be shown that for this simple case one solution is given by $P_1 = \sin^2 t$, $P_2 = \cos^2 t$, and $\text{Re}[c_1 {}^* c_2] = (1/2)\sin 2t$. At $t = 0$ the system is in the excited electronic state. When $t = \arccos[\epsilon_{BT}^{1/2}]$, the trajectory will either hop to surface 1 and be reinitialized, or remain on surface 2 and be reinitialized. The number of hop decisions over an interval of time, T, is thus $T/\arccos[\epsilon_{BT}^{1/2}]$, and the total number of hops that is expected to occur over this interval is given by $T\epsilon_{BT}/\arccos[\epsilon_{BT}^{1/2}]$. Clearly, as ϵ_{BT} approaches zero, the total number of hops also approaches zero, for any T.

This explanation reveals an important point in TSH calculations. The electronic coherence is important in the description of nonadiabatic dynamics, especially for systems with small values of $\dot{R} \cdot d_{12}(R)$. In these systems, the dynamics observed when electronic coefficients are reinitialized will be very different from the dynamics observed when coherence information is maintained. Further consideration of the type of argument in the previous paragraph eventually leads to the conclusion

that the rate of hopping must depend on the rate of change of the probabilities (as in the TFS algorithm) rather than the magnitude of the probabilities (as in the BT or GBT algorithm) and that the probabilities should not be reinitialized during the trajectory. In systems with large values of $\dot{\mathbf{R}}\cdot\mathbf{d}_{12}(\mathbf{R})$, the derivatives given in eqs C-3 and C-4 may be large even shortly after a reinitialization has occurred, and thus the coherence has a smaller effect on the dynamics. This is the kind of system for which the BT method was originally devised. This discussion shows why weakly coupled systems provide a critical test case for semiclassical methods.

References and Notes

(1) Tully, J. C. In *Modern Methods for Multidimensional Dynamics Computations in Chemistry*; Thompson, D. L., Ed.; World Scientific: Singapore, 1998; pp 34–72.

(2) Topaler, M. S.; Allison, T. C.; Schwenke, D. W.; Truhlar, D. G. *J. Chem. Phys.* **1998**, *109*, 3321; **1999**, *110*, 687(E).

(3) Meyer, H.-D.; Miller, W. H. *J. Chem. Phys.* **1979**, *70*, 3214.

(4) Blais, N. C.; Truhlar, D. G. *J. Chem. Phys.* **1983**, *79*, 1334.

(5) Tully, J. C. *J. Chem. Phys.* **1990**, *93*, 1061.

(6) Garciá-Vela, A.; Gerber, R. B.; Imre, D. G. *J. Chem. Phys.* **1992**, *97*, 7242.

(7) Tully, J. C. *Faraday Discuss. Chem. Soc.* **1998**, *110*, 407.

(8) Topaler, M. S.; Hack, M. D.; Allison, T. C.; Liu, Y.-P.; Mielke, S. L.; Schwenke, D. W.; Truhlar, D. G. *J. Chem. Phys.* **1997**, *106*, 8699.

(9) Topaler, M. S.; Allison, T. C.; Schwenke, D. W.; Truhlar, D. G. *J. Phys. Chem.* **1998**, *102*, 1666.

(10) Rosen, N.; Zener, C. *Phys. Rev.* **1932**, *40*, 502.

(11) Demkov, Yu. N. *J. Exp. Theor. Phys. (U. S. S. R.)* **1963**, *45*, 195 [English translation: *Sov. Phys. JETP* **1964**, *18*, 138].

(12) Demkov, Yu. N. *Dokl. Akad. Nauk SSSR* **1966**, *166*, 1076 [English translation: *Sov. Phys. Dokl.* **1966**, *11*, 138].

(13) Mielke, S. L.; Tawa, G. J.; Truhlar, D. G.; Schwenke, D. W. *Chem. Phys. Lett.* **1995**, *234*, 57.

(14) Mielke, S. L.; Truhlar, D. G.; Schwenke, D. W. *J. Phys. Chem.* **1995**, *99*, 16210.

(15) Sun, Y.; Kouri, D. J.; Truhlar, D. G.; Schwenke, D. W. *Phys. Rev. A* **1990**, *41*, 4857.

(16) Sun, Y.; Kouri, D. J.; Truhlar, D. G. *Nucl. Phys.* **1990**, *A508*, 41c.

(17) Tawa, G. J.; Mielke, S. L.; Truhlar, D. G.; Schwenke, D. W. *Adv. Mol. Vib. Col. Dyn.* **1993**, *2B*, 45.

(18) Tawa, G. J.; Mielke, S. L.; Truhlar, D. G.; Schwenke, D. W. *J. Am. Chem. Soc.* **1994**, *100*, 5751.

(19) Truhlar, D. G.; Muckerman, J. T. In *Atom-Molecule Collision Theory*; Bernstein, R. B., Ed.; Plenum: New York, 1979; p 505.

(20) Gordon, R. G. *J. Chem. Phys.* **1966**, *44*, 3083.

(21) Truhlar, D. G.; Reid, B. P.; Zurawski, D. E.; Gray, J. C. *J. Phys. Chem.* **1981**, *85*, 786.

(22) Herman, M. F. *J. Chem. Phys.* **1982**, *76*, 2949.

(23) Coker, D. F.; Xiao, L. *J. Chem. Phys.* **1995**, *102*, 496.

(24) See, for example: (a) Bowman, J. M.; Kuppermann, A. *Chem. Phys. Lett.* **1973**, *19*, 166; *J. Chem. Phys.* **1973**, *59*, 6524. (b) Schatz, G. S.; Bowman, J. M.; Kuppermann, A. *J. Chem. Phys.* **1975**, *63*, 674, 685. (c) Duff, J. W.; Truhlar, D. G. *Chem. Phys.* **1975**, *9*, 243. (d) Leasure, S. C.; Bowman, J. M. *Chem. Phys. Lett.* **1976**, *39*, 462. (e) Truhlar, D. G.; Merrick, J. A.; Duff, J. W. *J. Am. Chem. Soc.* **1976**, *98*, 6771. (f) Truhlar, D. G. *Int. J. Quantum Chem. Symp.* **1976**, *10*, 239. (g) Gray, J. C.; Truhlar, D. G.; Clemens, L.; Duff, J. W.; Chapman, F. M., Jr.; Morrell, G. O.; Hayes, E. F. *J. Chem. Phys.* **1978**, *69*, 240. (h) Gray, J. C.; Garrett, B. C.; Truhlar, D. G. *J. Chem. Phys.* **1979**, *70*, 5921. (i) Ron, S.; Baer, M.; Pollak, E. *J. Chem. Phys.* **1978**, *68*, 4413.

(25) Ashton, C. J.; Muckerman, J. T.; Schubert, F. E. *J. Chem. Phys.* **1984**, *81*, 5786.

(26) (a) Blais, N. C.; Truhlar, D. G.; Garrett, B. C. *J. Chem. Phys.* **1983**, *78*, 4419. (b) Steckler, S.; Truhlar, D. G.; Garrett, B. C.; Blais, N. C.; Walker, R. B. *J. Chem. Phys.* **1984**, *81*, 5700. (c) Schatz, G. C.; *J. Chem. Phys.* **1985**, *83*, 3441. (d) Miller, J. A. *J. Chem. Phys.* **1986**, *84*, 6170. (e) Mandy, M. E.; Martin, P. G. *J. Phys. Chem.* **1991**, *95*, 8726.

(27) Schwenke, D. W.; Volobuev, Y. L.; Mielke, S. L.; Tawa, G. J.; Chatfield, D. C.; Sun, Y.; Haug, K.; Allison, T. C.; Friedman, R. S.; Zhao, M.; Halvick, P.; Hack, M. D.; Truhlar, D. G. VP—version 18.7, University of Minnesota, Minneapolis, 1998.

(28) Topaler, M. S.; Hack, M. D.; Volobuev, Y. L.; Allison, T. C.; Liu, Y.-P.; Blais, N. C.; Truhlar, D. G. TSH—version 5.3, University of Minnesota, Minneapolis, 1998.

(29) Press, W. K.; Teukolsky, S. A.; Vetterling, W. T.; Flannery, B. P. *Numerical Recipes*, 2nd ed.; Cambridge University Press: Cambridge, 1982; pp 718ff.

(30) Hack, M. D.; Jasper A.; Volobuev, Y. L.; Schwenke, D. W.; Truhlar, D. G. To be published.

(31) Mead, C. A.; Truhlar, D. G. *J. Chem. Phys.* **1982**, *77*, 6090.

(32) Preston, R. K.; Tully, J. C. *J. Chem. Phys.* **1971**, *54*, 4297.

(33) Tully, J. C. *J. Chem. Phys.* **1973**, *59*, 5122; *J. Chem. Phys.* **1974**, *60*, 3042.

Supporting information for

Are Semiclassical Methods Accurate for Electronically Nonadiabatic Transitions Between Weakly Coupled Potential Energy Surfaces?

Yuri L. Volobuev, Michael D. Hack, and Donald G. Truhlar

Department of Chemistry and Supercomputer Institute, University of Minnesota,

Minneapolis, MN 55455-0431

This supporting information contains full tables of numerical results to support the article printed in *Journal of Physical Chemistry A.*

Contents

Date of preparation of supporting information: Jan. 29, 1998

Page 1 of 21

Table S-1. Nonreactive de-excitation probabilities and unsigned mean errors calculated by quantum scattering calculations and by SCP methods with linear smooth sampling for Br* + $H_2(v, j) \rightarrow$ Br + H_2, summed over final vibrational-rotational states, at $E_{tot} = 1.3$ eV

(v, j)	Quantum	Meyer-Miller		Ehrenfest	
		ENC	EC	ENC	EC
(0,0)	1.7e-3	2.1e-2	2.1e-2	1.2e-3	1.2e-3
(0,2)	4.4e-3	2.3e-2	2.4e-2	8.8e-4	8.8e-4
(0,4)	8.0e-3	2.6e-2	2.7e-2	4.5e-3	4.5e-3
(0,6)	2.0e-3	2.6e-2	2.8e-2	1.1e-3	1.1e-3
(0,8)	2.1e-2	3.5e-2	3.8e-2	2.7e-3	2.7e-3
(1,0)	2.1e-6	2.1e-2	2.2e-2	1.4e-3	1.4e-3
(1,2)	9.5c-6	2.4c-3	2.4e-3	2.0e-5	2.0e-5
ΔP^{quench}		1.7e-2	1.8e-2	4.1e-3	4.1e-3

Table S-2. State-to-state quenching probability for $Br + H_2$ $(v', j') \rightarrow Br^* + H_2(v, j)$ calculated by the Ehrenfest method with energy-non-conserving linear smooth sampling at $E_{tot} = 1.3$ eV and state-selected quenching probabilities for $Br^* + H_2$ $(v, j) \rightarrow Br + H_2$ (all v', all j') calculated by the reverse Ehrenfest-LSS-ENC method

(v', j')	(v, j)						
	(0,0)	(0,2)	(0,4)	(0,6)	(0,8)	(1,0)	(1,2)
(0,0)	2.64e-4	2.70e-4	4.51e-5	1.97e-5	7.38e-8	7.32e-6	2.10e-5
(0,2)	3.21e-4	9.85e-4	2.78e-4	6.14e-5	1.06e-6	2.47e-5	1.27e-4
(0,4)	5.27e-5	3.85e-4	6.74e-4	1.42e-4	1.11e-5	2.37e-5	2.70e-4
(0,6)	7.50e-7	2.08e-5	2.63e-4	4.87e-4	1.06e-4	4.83e-6	2.08e-4
(0,8)	3.72e-7	1.10e-5	1.68e-5	1.99e-4	1.20e-3	9.40e-6	9.23e-5
(0,10)	0	0	0	0	2.01e-4	0	0
(1,0)	2.66e-5	3.89e-5	7.10e-6	1.28e-6	0	1.15e-3	1.01e-3
(1,2)	6.62e-5	2.62e-4	2.64e-4	2.19e-4	8.39e-5	1.43e-3	2.55e-3
(1,4)	6.18e-7	2.80e-5	2.40e-4	5.93e-4	1.04e-4	8.52e-5	9.08e-4
(1,6)	0	0	3.85e-6	4.90e-4	1.41e-4	0	0
(1,8)	0	0	0	6.48e-9	5.34e-5	0	0
(2,0)	0	0	0	0	0	1.97e-4	4.02e-5
$P_{(v,j)}^{quench}$	7.32e-4	2.00e-3	1.79e-3	2.21e-3	1.90e-3	2.93e-3	5.23e-3

Table S-3. State-to-state quenching probability for Br + H_2 $(v', j') \rightarrow$ Br* + $H_2(v, j)$ calculated by the Ehrenfest method with energy-conserving linear smooth sampling at $E_{tot} = 1.3$ eV and state-selected quenching probabilities for Br* + H_2 $(v, j) \rightarrow$ Br + H_2 (all v', all j') calculated by the reverse Ehrenfest-LSS-EC method

(v', j')	(v, j)						
	(0,0)	(0,2)	(0,4)	(0,6)	(0,8)	(1,0)	(1,2)
(0,0)	2.64e-4	2.70e-4	4.51e-5	1.97e-5	7.38e-8	7.38e-6	2.14e-5
(0,2)	3.21e-4	9.85e-4	2.78e-4	6.14e-5	1.06e-6	2.47e-5	1.28e-4
(0,4)	5.27e-5	3.85e-4	6.74e-4	1.42e-4	1.11e-5	2.41e-5	2.79e-4
(0,6)	7.50e-7	2.08e-5	2.63e-4	4.87e-4	1.06e-4	5.50e-6	2.85e-4
(0,8)	3.72e-7	1.10e-5	1.68e-5	1.99e-4	1.20e-3	1.13e-5	1.08e-4
(0,10)	0	0	0	0	2.17e-4	0	0
(1,0)	2.66e-5	3.89e-5	7.14e-6	1.28e-6	0	1.15e-3	1.01e-3
(1,2)	6.62e-5	2.62e-4	2.65e-4	2.20e-4	8.39e-5	1.44e-3	2.60e-3
(1,4)	6.18e-7	2.81e-5	2.41e-4	5.95e-4	1.04e-4	9.06e-5	1.08e-3
(1,6)	0	0	3.89e-6	4.97e-4	1.43e-4	0	0
(1,8)	0	0	0	6.53e-9	5.39e-5	0	0
(2,0)	0	0	0	0	0	2.48e-4	5.48e-5
$P_{(v,j)}^{quench}$	7.32e-4	2.00e-3	1.79e-3	2.22e-3	1.92e-3	3.00e-3	5.57e-3

Table S-4. State-to-state quenching probability for Br + H$_2$ $(v', j') \rightarrow$ Br* + H$_2(v, j)$ calculated by the

TFS method with energy-non-conserving histogram sampling at E_{tot} = 1.3 eV and state-selected quenching probabilities for

Br* + H$_2$ $(v, j) \rightarrow$ Br + H$_2$ (all v', all j') calculated by the reverse TFS-H-ENC method

(v', j')	(v, j)						
	(0,0)	(0,2)	(0,4)	(0,6)	(0,8)	(1,0)	(1,2)
(0,0)	3.33e-4	4.00e-4	0	0	0	6.67e-5	0
(0,2)	1.33e-4	1.40e-3	2.00e-4	6.67e-5	0	0	0
(0,4)	0	7.33e-4	1.00e-3	6.67e-5	0	6.67e-5	2.67e-4
(0,6)	0	0	4.00e-4	4.67e-4	2.00e-4	0	1.33e-4
(0,8)	0	0	0	1.33e-4	1.40e-3	0	0
(0,10)	0	0	0	0	6.67e-5	0	0
(1,0)	1.33e-4	6.67e-5	0	0	0	1.80e-3	6.67e-4
(1,2)	0	8.00e-4	2.67e-4	2.00e-4	6.67e-5	1.13e-3	1.27e-3
(1,4)	0	0	6.00e-4	4.67e-4	6.67e-5	0	8.00e-4
(1,6)	0	0	0	1.93e-3	6.67e-5	0	0
(1,8)	0	0	0	0	0	0	0
(2,0)	0	0	0	0	0	6.67e-5	0
$P_{(v,j)}^{quench}$	5.99e-4	3.40e-3	2.47e-3	3.33e-3	1.87e-3	3.13e-3	3.14e-3

Table S-5. State-to-state quenching probability for $Br + H_2 (v', j') \rightarrow Br^* + H_2(v, j)$ calculated by the TFS method with energy-conserving histogram sampling at $E_{tot} = 1.3$ eV and state-selected quenching probabilities for $Br^* + H_2 (v, j) \rightarrow Br + H_2$ (all v', all j') calculated by the reverse TFS-H-EC method

(v', j')	(v, j)						
	(0,0)	(0,2)	(0,4)	(0,6)	(0,8)	(1,0)	(1,2)
(0,0)	3.33e-4	4.00e-4	0	0	0	6.67e-5	0
(0,2)	1.33e-4	1.40e-3	2.00e-4	6.67e-5	0	0	0
(0,4)	0	7.33e-4	1.00e-3	6.67e-5	0	6.67e-5	2.67e-4
(0,6)	0	0	4.00e-4	4.67e-4	2.00e-4	0	1.33e-4
(0,8)	0	0	0	1.33e-4	1.40e-3	0	0
(0,10)	0	0	0	0	6.67e-5	0	0
(1,0)	1.33e-4	6.67e-5	0	0	0	1.80e-3	6.67e-4
(1,2)	0	8.00e-4	2.67e-4	2.00e-4	6.67e-5	1.13e-3	1.27e-3
(1,4)	0	0	6.00e-4	4.67e-4	6.67e-5	0	8.00e-4
(1,6)	0	0	0	1.93e-3	6.67e-5	0	0
(1,8)	0	0	0	0	0	0	0
(2,0)	0	0	0	0	0	6.67e-5	0
$P^{quench}_{(v,j)}$	5.99e-4	3.40e-3	2.47e-3	3.33e-3	1.87e-3	3.13e-3	3.14e-3

Table S-6. State-to-state quenching probability for $Br + H_2 (v', j') \rightarrow Br^* + H_2(v, j)$ calculated by the TFS method with energy-non-conserving linear smooth sampling at $E_{tot} = 1.3$ eV and state-selected quenching probabilities for $Br^* + H_2 (v, j) \rightarrow Br + H_2$ (all v', all j') calculated by the reverse TFS-LSS-ENC method

(v', j')	(v, j)						
	(0,0)	(0,2)	(0,4)	(0,6)	(0,8)	(1,0)	(1,2)
(0,0)	3.62e-4	3.10e-4	5.40e-5	0	0	6.74e-5	6.23e-6
(0,2)	2.63e-4	1.14e-3	2.48e-4	7.51e-5	0	5.26e-6	3.88e-5
(0,4)	7.29e-5	6.43e-4	9.02e-4	8.81e-5	0	4.20e-5	2.64e-4
(0,6)	0	7.19e-5	3.70e-4	4.62e-4	1.46e-4	0	8.29e-5
(0,8)	0	7.78e-6	2.17e-5	2.75e-4	1.13e-3	0	1.06e-5
(0,10)	0	0	0	0	7.22e-5	0	0
(1,0)	4.40e-4	2.83e-4	1.38e-5	0	0	1.33e-3	5.89e-4
(1,2)	3.90e-4	7.33e-4	4.26e-4	1.62e-4	6.51e-5	7.95e-4	1.10e-3
(1,4)	1.17e-5	1.75e-4	5.48e-4	5.21e-4	5.97e-5	3.66e-5	5.54e-4
(1,6)	0	5.08e-6	2.12e-4	1.25e-3	2.63e-4	0	3.72e-5
(1,8)	0	0	0	0	0	0	0
(2,0)	8.78e-6	0	0	0	0	5.79e-5	0
$P_{(v,j)}^{quench}$	1.55e-3	3.37e-3	2.80e-3	2.83e-3	1.74e-3	2.33e-3	2.68e-3

Table S-7. State-to-state quenching probability for $Br + H_2 (v', j') \rightarrow Br^* + H_2(v, j)$ calculated by the TFS method with energy-conserving linear smooth sampling at $E_{tot} = 1.3$ eV and state-selected quenching probabilities for $Br^* + H_2 (v, j) \rightarrow Br + H_2$ (all v', all j') calculated by the reverse TFS-LSS-EC method

(v', j')	(v, j)						
	(0,0)	(0,2)	(0,4)	(0,6)	(0,8)	(1,0)	(1,2)
(0,0)	3.62e-4	3.10e-4	5.42e-5	0	0	6.74e-5	6.23e-6
(0,2)	2.63e-4	1.15e-3	2.69e-4	7.54e-5	0	5.26e-6	4.05e-5
(0,4)	7.29e-5	6.95e-4	1.09e-3	1.24e-4	0	4.20e-5	3.14e-4
(0,6)	0	9.47e-5	4.98e-4	4.83e-4	1.46e-4	0	1.13e-4
(0,8)	0	1.34e-5	3.73e-5	3.34e-4	1.26e-3	0	1.83e-5
(0,10)	0	0	0	0	2.00e-4	0	0
(1,0)	4.40e-4	2.87e-4	1.55e-5	0	0	1.33e-3	5.91e-4
(1,2)	3.90e-4	8.00e-4	6.97e-4	2.42e-4	6.61e-5	7.95e-4	1.21e-3
(1,4)	1.17e-5	2.23e-4	9.64e-4	6.81e-4	6.93e-5	3.66e-5	6.81e-4
(1,6)	0	1.27e-5	4.76e-4	1.94e-3	3.48e-4	0	8.99e-5
(1,8)	0	0	0	0	0	0	0
(2,0)	8.78e-6	0	0	0	0	5.79e-5	0
$P_{(v,j)}^{quench}$	1.55e-3	3.59e-3	4.10e-3	3.88e-3	2.09e-3	2.33e-3	3.06e-3

Table S-8. Nonreactive de-excitation (i.e., quenching) probabilities and unsigned mean errors calculated by quantum scattering calculations and by the reverse methods for Br* + $H_2(v, j)$ at $E_{tot} = 1.3$ eV

| (v, j) | Quantum | Reverse TFS | | | | Reverse Ehrenfest | |
| | | Histogram | | LSS | | LSS | |
		ENC	EC	ENC	EC	ENC	EC
(0,0)	1.7e-3	6.0e-4	6.0e-4	1.5e-3	1.5e-3	7.3e-4	7.3e-4
(0,2)	4.4e-3	3.4e-3	3.4e-3	3.4e-3	3.6e-3	2.0e-3	2.0e-3
(0,4)	8.0e-3	2.5e-3	2.5e-3	2.8e-3	4.1e-3	1.8e-3	1.8e-3
(0,6)	2.0e-3	3.3e-3	3.3e-3	2.8e-3	3.9e-3	2.2e-3	2.2e-3
(0,8)	2.1e-2	1.9e-3	1.9e-3	1.7e-3	2.1e-3	1.9e-3	1.9e-3
(1,0)	2.1e-6	3.1e-3	3.1e-3	2.3e-3	2.3e-3	2.9e-3	3.0e-3
(1,2)	9.5e-6	3.1e-3	3.1e-3	2.7e-3	3.1e-3	5.2e-3	5.6e-3
ΔP^{quench}		5.0e-3	5.0e-3	4.6e-3	4.5e-3	5.4e-3	5.4e-3

Table S-9. Nonadiabatic probabilities and unsigned mean errors calculated by quantum scattering calculations and by SCP methods with linear smooth sampling for Br* + $H_2(v, j)$ at $E_{tot} = 1.3\,eV$

(v, j)	Quantum	Meyer-Miller		Ehrenfest	
		ENC	EC	ENC	EC
(0,0)	2.3e-3	2.1e-2	2.1e-2	1.2e-3	1.2e-3
(0,2)	5.8e-3	2.3e-2	2.4e-2	8.8e-4	8.8e-4
(0,4)	9.3e-3	2.6e-2	2.7e-2	4.5e-3	4.5e-3
(0,6)	2.2e-3	2.6e-2	2.8e-2	1.1e-3	1.1e-3
(0,8)	2.1e-2	3.5e-2	3.8e-2	2.7e-3	2.7e-3
(1,0)	2.1e-6	2.1e-2	2.2e-2	1.4e-3	1.4e-3
(1,2)	9.5e-6	2.4e-3	2.4e-3	2.0c-5	2.0c-5
ΔP^{nonad}		1.6e-2	1.7e-2	4.6e-3	4.6e-3

Table S-10. Nonadiabatic probabilities and unsigned mean errors calculated by quantum scattering calculations and by SCP methods with linear smooth sampling for Br* + $H_2(v, j)$ at $E_{tot} = 1.5\,eV$

(v, j)	Quantum	Meyer-Miller		Ehrenfest	
		ENC	EC	ENC	EC
(0,0)	2.1e-3	8.2e-3	8.2e-3	6.4e-4	6.4e-4
(0,2)	2.8e-3	1.6e-2	1.6e-2	2.5e-3	2.5e-3
(0,4)	6.1e-3	4.0e-2	4.0e-2	4.4e-3	4.4e-3
(0,6)	7.3e-3	2.5e-2	2.6e-2	2.6e-3	2.6e-3
(0,8)	1.0e-3	3.3e-2	3.5e-2	1.5e-3	1.6e-3
(0,10)	1.9e-7	1.6e-3	1.6e-3	8.1e-6	5.9e-1
(1,0)	4.1e-3	3.9e-2	4.5e-2	7.3e-3	7.4e-3
(1,2)	1.6e-2	9.4e-2	1.2e-1	1.2e-2	1.3e-2
(1,4)	4.2e-3	6.2e-2	7.2e-2	2.0e-2	9.1e-1
ΔP^{nonad}		3.1e-02	3.6e-02	3.5e-03	1.7e-01

Table S-11. Nonadiabatic probabilities and mean unsigned errors calculated by quantum scattering calculations and by the TFS method for $Br^* + H_2(v, j)$

| (v, j) | $E_{tot} = 1.3$ eV | | | $E_{tot} = 1.5$ eV | | |
| | | TFS[a] | | | TFS[a] | |
	Quantum	ENC	EC	Quantum	ENC	EC
(0,0)	2.3e-3	2.2e-3	1.9e-3	2.1e-3	1.5e-3	1.5e-3
(0,2)	5.8e-3	2.7e-3	2.3e-3	2.8e-3	4.8e-3	4.7e-3
(0,4)	9.3e-3	8.1e-3	7.7e-3	6.1e-3	8.2e-3	8.1e-3
(0,6)	2.2e-3	3.9e-3	3.7e-3	7.3e-3	5.8e-3	6.1e-3
(0,8)	2.1e-2	4.5e-3	4.5e-3	1.0e-3	4.0e-3	4.2e-3
(0,10) [b]	–	–	–	1.9e-7	1.6e-4	1.0e+0
(1,0)	2.1e-6	2.3e-3	2.2e-3	4.1e-3	8.2e-3	7.9e-3
(1,2)	9.5e-6	5.5e-4	3.3e-4	1.6e-2	1.7e-2	1.5e-2
(1,4) [b]	–	–	–	4.2e-3	2.4e-2	7.5e-1
ΔP^{nonad}		3.7e-3	3.8e-3		3.8e-3	2.0e-1

[a]For the TFS method, the histogram and linear smooth sampling methods give identical reactive and quenching probabilities

[b]At $E_{tot} = 1.3$ eV states (0,10) and (1,4) are closed

Table S-12. Nonadiabatic probabilities and unsigned mean errors calculated by quantum scattering calculations and by the reverse methods for Br* + $H_2(v, j)$ at $E_{tot} = 1.3$ eV

(v, j)	Quantum	Reverse TFS				Reverse Ehrenfest	
		Histogram		LSS		LSS	
		ENC	EC	ENC	EC	ENC	EC
(0,0)	2.3e-3	6.0e-4	6.0e-4	1.6e-3	1.6e-3	7.4e-4	7.4e-4
(0,2)	5.8e-3	3.5e-3	3.5e-3	3.9e-3	4.3e-3	2.1e-3	2.1e-3
(0,4)	9.3e-3	3.0e-3	3.0e-3	3.5e-3	5.4e-3	2.2e-3	2.2e-3
(0,6)	2.2e-3	4.1e-3	4.1e-3	3.4e-3	4.6e-3	2.7e-3	2.7e-3
(0,8)	2.1e-2	1.9e-3	1.9e-3	1.7e-3	2.1e-3	2.0e-3	2.0e-3
(1,0)	2.1e-6	3.1e-3	3.1e-3	2.3e-3	2.3e-3	3.0e-3	3.1e-3
(1,2)	9.5e-6	5.1e-3	5.1e-3	4.1e-3	5.0e-3	7.6e-3	8.4e-3
ΔP^{nonad}		5.7e-3	5.7e-3	5.1e-3	5.0e-3	6.1e-3	6.3e-3

Table S-13. Reaction probabilities and mean unsigned errors calculated by quantum scattering calculations and by the TFS method for the reaction of Br* with $H_2(v, j)$

| (v, j) | $E_{tot} = 1.3$ eV | | | $E_{tot} = 1.5$ eV | | |
| | | TFS[a] | | | TFS[a] | |
	Quantum	ENC	EC	Quantum	ENC	EC
(0,0)	6.4e-4	2.2e-4	2.2e-4	6.8e-4	5.4e-4	5.4e-4
(0,2)	1.4e-3	5.2e-4	5.2e-4	1.3e-3	9.8e-4	9.8e-4
(0,4)	1.3e-3	1.1e-3	1.1e-3	1.7e-3	1.7e-3	1.8e-3
(0,6)	2.3e-4	7.0e-4	7.0e-4	9.9e-4	1.8e-3	2.0e-3
(0,8)	2e-9	1.5e-4	1.5e-4	5.7e-4	7.6e-4	7.6e-4
(0,10) [b]	–	–	–	2.8e-8	8.0e-6	8.0e-6
(1,0)	4e-10	4.4e-5	4.4e-5	2.7e-3	9.2e-4	9.2e-4
(1,2)	1e-10	1.4e-5	1.4e-5	3.0e-3	4.1e-3	4.1e-3
(1,4) [b]	–	–	–	2.1e-5	4.2e-3	4.2e-3
ΔP^{react}		3.2e-4	3.2e-4		9.4e-4	9.8e-4

[a]For the TFS method, the histogram and linear smooth sampling methods give identical reactive and quenching probabilities

[b]At $E_{tot} = 1.3$ eV states (0,10) and (1,4) are closed

Table S-14. State-to-state reaction probability for the reaction $H + HBr(v', j') \rightarrow Br^* + H_2(v, j)$ calculated by the Ehrenfest method with energy-non-conserving linear smooth sampling at $E_{tot} = 1.3$ eV and state-selected reaction probabilities for $Br^* + H_2(v, j) \rightarrow H + HBr$ (all v', all j') calculated by the reverse Ehrenfest-LSS-ENC method

(v', j')	(v, j)						
	(0,0)	(0,2)	(0,4)	(0,6)	(0,8)	(1,0)	(1,2)
(0,0)	7.64e-7	3.01e-6	1.34e-5	1.55e-6	1.68e-7	2.78e-6	9.73e-5
(0,1)	6.44e-7	4.92e-6	2.73e-5	5.06e-6	3.16e-7	2.80e-6	1.84e-4
(0,2)	7.77e-7	7.10e-6	4.19e-5	1.43e-5	4.86e-7	2.42e-6	2.26e-4
(0,3)	5.93e-7	6.01e-6	3.92e-5	2.53e-5	4.87e-7	3.47e-6	2.16e-4
(0,4)	5.81e-7	4.66e-6	2.77e-5	3.05e-5	1.16e-6	3.18e-6	1.60e-4
(0,5)	4.20e-7	2.93e-6	2.05e-5	3.33e-5	2.95e-6	4.71e-6	1.15e-4
(0,6)	2.26e-7	2.09e-6	1.76e-5	3.73e-5	6.44e-6	6.39e-6	7.64e-5
(0,7)	3.63e-8	1.33e-6	1.61e-5	3.50e-5	8.95e-6	6.39e-6	5.45e-5
(0,8)	5.72e-8	1.13e-6	1.17e-5	2.42e-5	6.99e-6	1.35e-6	2.33e-5
(0,9)	2.79e-8	1.04e-6	4.12e-6	1.50e-5	2.17e-5	2.05e-6	1.82e-5
(0,10)	0	0	0	0	0	0	0
(0,11)	0	0	0	0	0	0	0
$P_{(v,j)}^{react}$	8.25e-6	6.84e-5	4.39e-4	4.43e-4	9.93e-5	7.11e-5	2.34e-3

Table S-15. State-to-state reaction probability for the reaction $H + HBr(v', j') \rightarrow Br^* + H_2(v, j)$ calculated by the Ehrenfest method with energy-conserving linear smooth sampling at $E_{tot} = 1.3$ eV and state-selected reaction probabilities for $Br^* + H_2(v, j) \rightarrow H + HBr$ (all v', all j') calculated by the reverse Ehrenfest-LSS-EC method

(v', j')	(v, j)						
	(0,0)	(0,2)	(0,4)	(0,6)	(0,8)	(1,0)	(1,2)
(0,0)	7.64e-7	3.02e-6	1.34e-5	1.55e-6	1.69e-7	3.08e-6	1.14e-4
(0,1)	6.44e-7	4.93e-6	2.73e-5	5.07e-6	3.16e-7	3.36e-6	2.17e-4
(0,2)	7.77e-7	7.11e-6	4.20e-5	1.43e-5	4.86e-7	2.98e-6	2.70e-4
(0,3)	5.93e-7	6.02e-6	3.93e-5	2.53e-5	4.87e-7	3.98e-6	2.66e-4
(0,4)	5.81e-7	4.67e-6	2.78e-5	3.05e-5	1.17e-6	3.63e-6	2.03e-4
(0,5)	4.20e-7	2.94e-6	2.05e-5	3.33e-5	2.95e-6	4.95e-6	1.51e-4
(0,6)	2.26e-7	2.09e-6	1.76e-5	3.74e-5	6.45e-6	6.63e-6	9.57e-5
(0,7)	3.63e-8	1.33e-6	1.62e-5	3.51e-5	8.95e-6	6.60e-6	6.15e-5
(0,8)	5.72e-8	1.13e-6	1.17e-5	2.42e-5	7.01e-6	1.59e-6	2.60e-5
(0,9)	2.79e-8	1.04e-6	4.13e-6	1.50e-5	2.18e-5	2.49e-6	2.12e-5
(0,10)	0	0	0	0	0	0	0
(0,11)	0	0	0	0	0	0	0
$P^{react}_{(v,j)}$	8.25e-6	6.86e-5	4.40e-4	4.43e-4	9.96e-5	7.86e-5	2.85e-3

Table S-16. State-to-state reaction probability for the reaction $H + HBr(v', j') \rightarrow Br^* + H_2(v, j)$ calculated by the TFS method with energy-non-conserving histogram sampling at $E_{tot} = 1.3$ eV and state-selected reaction probabilities for $Br^* + H_2(v, j) \rightarrow H + HBr$ (all v', all j') calculated by the reverse TFS-H-ENC method

(v', j')	(v, j)						
	(0,0)	(0,2)	(0,4)	(0,6)	(0,8)	(1,0)	(1,2)
(0,0)	0	0	0	0	0	0	2.00e-4
(0,1)	0	0	0	0	0	0	6.67e-5
(0,2)	0	0	0	0	0	0	6.67e-5
(0,3)	0	6.67e-5	6.67e-5	6.67e-5	0	0	2.67e-4
(0,4)	0	0	6.67e-5	6.67e-5	0	0	2.00e-4
(0,5)	0	0	6.67e-5	0	0	0	2.00e-4
(0,6)	0	0	6.67e-5	1.33e-4	0	0	0
(0,7)	0	0	0	6.67e-5	0	0	0
(0,8)	0	0	0	0	0	0	0
(0,9)	0	0	0	6.67e-5	0	0	0
(0,10)	0	0	0	0	0	0	0
(0,11)	0	0	0	0	0	0	0
$P_{(v,j)}^{react}$	0	1.33e-4	5.34e-4	8.00e-4	0	0	2.00e-3

Table S-17. State-to-state reaction probability for the reaction $H + HBr(v', j') \rightarrow Br^* + H_2(v, j)$ calculated by the TFS method with energy-conserving histogram sampling at $E_{tot} = 1.3$ eV and state-selected reaction probabilities for $Br^* + H_2(v, j) \rightarrow H + HBr$ (all v', all j') calculated by the reverse TFS-H-EC method

(v', j')	(v, j)						
	(0,0)	(0,2)	(0,4)	(0,6)	(0,8)	(1,0)	(1,2)
(0,0)	0	0	0	0	0	0	2.00e-4
(0,1)	0	0	0	0	0	0	6.67e-5
(0,2)	0	0	0	0	0	0	6.67e-5
(0,3)	0	6.67e-5	6.67e-5	6.67e-5	0	0	2.67e-4
(0,4)	0	0	6.67e-5	6.67e-5	0	0	2.00e-4
(0,5)	0	0	6.67e-5	0	0	0	2.00e-4
(0,6)	0	0	6.67e-5	1.33e-4	0	0	0
(0,7)	0	0	0	6.67e-5	0	0	0
(0,8)	0	0	0	0	0	0	0
(0,9)	0	0	0	6.67e-5	0	0	0
(0,10)	0	0	0	0	0	0	0
(0,11)	0	0	0	0	0	0	0
$P^{react}_{(v,j)}$	0	1.33e-4	5.34e-4	8.00e-4	0	0	2.00e-3

Table S-18. State-to-state reaction probability for the reaction $H + HBr(v', j') \rightarrow Br^* + H_2(v, j)$ calculated by the TFS method with energy-non-conserving linear smooth sampling at $E_{tot} = 1.3$ eV and state-selected reaction probabilities for $Br^* + H_2(v, j) \rightarrow H + HBr$ (all v', all j') calculated by the reverse TFS-LSS-ENC method

(v', j')	(v, j)						
	(0,0)	(0,2)	(0,4)	(0,6)	(0,8)	(1,0)	(1,2)
(0,0)	6.38e-8	4.12e-5	3.24e-5	0	0	3.37e-7	1.31e-4
(0,1)	0	2.20e-5	1.26e-5	0	0	0	5.65e-5
(0,2)	0	2.12e-5	2.24e-5	0	0	0	4.74e-5
(0,3)	4.95e-6	6.06e-5	6.30e-5	4.19e-5	0	3.72e-6	2.07e-4
(0,4)	0	5.52e-5	8.21e-5	3.69e-5	0	0	1.44e-4
(0,5)	0	5.01e-5	4.30e-5	0	0	0	1.08e-4
(0,6)	0	1.01e-5	1.03e-4	1.22e-4	0	0	3.07e-5
(0,7)	0	0	1.14e-5	3.03e-5	0	0	0
(0,8)	0	0	0	0	0	0	0
(0,9)	0	0	0	4.07e-5	3.90e-6	0	0
(0,10)	0	0	0	0	0	0	0
(0,11)	0	0	0	0	0	0	0
$P^{react}_{(v,j)}$	1.00e-5	5.21e-4	7.40e-4	5.44e-4	7.80e-6	8.11e-6	1.45e-3

Table S-19. State-to-state reaction probability for the reaction $H + HBr(v', j') \rightarrow Br^* + H_2(v, j)$ calculated by the TFS method with energy-conserving linear smooth sampling at $E_{tot} = 1.3$ eV and state-selected reaction probabilities for $Br^* + H_2(v, j) \rightarrow H + HBr$ (all v', all j') calculated by the reverse TFS-LSS-EC method

(v', j')	(v, j)						
	(0,0)	(0,2)	(0,4)	(0,6)	(0,8)	(1,0)	(1,2)
(0,0)	6.38e-8	5.13e-5	5.80e-5	0	0	3.37e-7	1.57e-4
(0,1)	0	2.81e-5	2.83e-5	0	0	0	7.69e-5
(0,2)	0	3.08e-5	3.58e-5	0	0	0	6.67e-5
(0,3)	4.95e-6	6.76e-5	1.35e-4	7.20e-5	0	3.72e-6	2.50e-4
(0,4)	0	7.88e-5	1.27e-4	4.05e-5	0	0	2.20e-4
(0,5)	0	6.70e-5	5.84e-5	0	0	0	1.41e-4
(0,6)	0	1.89e-5	1.92e-4	1.34e-4	0	0	5.53e-5
(0,7)	0	0	1.82e-5	4.84e-5	0	0	0
(0,8)	0	0	0	0	0	0	0
(0,9)	0	0	0	6.08e-5	5.84e-6	0	0
(0,10)	0	0	0	0	0	0	0
(0,11)	0	0	0	0	0	0	0
$P^{react}_{(v,j)}$	1.00e-5	6.85e-4	1.31e-3	7.11e-4	1.17e-5	8.11e-6	1.93e-3

Table S-20. Reaction probabilities and unsigned mean errors calculated by quantum scattering calculations and by the reverse methods for $Br^* + H_2(v, j)$ at $E_{tot} = 1.3$ eV

| (v, j) | Quantum | Reverse TFS | | | | Reverse Ehrenfest | |
| | | Histogram | | LSS | | LSS | |
		ENC	EC	ENC	EC	ENC	EC
(0,0)	6.4e-4	0	0	1.0e-5	1.0e-5	8.3e-6	8.3e-6
(0,2)	1.4e-3	1.3e-4	1.3e-4	5.2e-4	6.9e-4	6.8e-5	6.9e-5
(0,4)	1.3e-3	5.3e-4	5.3e-4	7.4e-4	1.3e-3	4.4e-4	4.4e-4
(0,6)	2.3e-4	8.0e-4	8.0e-4	5.4e-4	7.1e-4	4.4e-4	4.4e-4
(0,8)	2e-9	0	0	7.8e-6	1.2e-5	9.9e-5	1.0e-4
(1,0)	4e-10	0	0	8.1e-6	8.1e-6	7.1e-5	7.9e-5
(1,2)	1e-10	2.0e-3	2.0e-3	1.4e-3	1.9e-3	2.3e-3	2.9e-3
ΔP^{react}		7.6e-4	7.6e-4	5.6e-4	5.6e-4	8.0e-4	8.7e-4